UMYU Scientifica, Vol. 1 NO. 1, September 2022, Pp 155 – 165
https://doi.org/10.56919/usci.1122.020
ISSN: 2955 – 1145 (print); 2955 – 1153 (online)
A periodical of the Faculty of Natural and Applied Sciences, UMYU, Katsina

ORIGINAL RESEARCH ARTICLE

Study on Adsorption of Alizarin Red S and Eriochrome Black T Dyes by Untreated Typha Grass as a Low Cost Adsorbent

Ayuba, Abdullahi Muhammad and Sani, Musa
Department of Pure and Industrial Chemistry, Faculty of Physical Sciences, Bayero University, Kano, Nigeria

ABSTRACT
The purpose of this investigation was to study the adsorptive potential of untreated typha grass (UTG) using a batch system under control conditions to decolorize Alizarin Red S (ARS) and Eriochrome Black T (EBT) anionic toxic dyes from synthetic aqueous solution. In this regard, the impact of various experimental parameters namely, contact time, adsorbent dose, initial dye concentration, pH, and temperature were assessed and optimized. The adsorbent was characterized using Fourier transformed infrared (FTIR) spectroscopy, scanning electron microscopy (SEM), and point of zero charge (PZC) analysis. The maximum adsorption rates of ARS and EBT onto UTG were determined to be 49.92 mg/g and 47.43 mg/g, respectively, at equilibrium. In comparison to previous models evaluated, removal of both ARS and EBT by the UTG demonstrated that the data had a strong fit with pseudo-second-order kinetic and Freundlich adsorption isotherms. The contact time for both dyes was optimised at 15 minutes, while the pH for ARS and EBT were attained at 8 and 2 respectively. However, based on the established results of various parameters in this study, the adsorptive removal of ARS and EBT by UTG was a favourable process. The Van't Hoff plot was used to calculate the thermodynamic quantities of the adsorption process, including ΔG, ΔH and ΔS. The outcomes showed that the process was both spontaneous and thermodynamically possible. From the parameters tested, EBT was found to be better adsorbed onto UTG than ARS. Even though both dyes are anionic in nature, but EBT has additional diazo and nitro functional groups than the hydroxyl and sulphate functional groups present in ARS. This might be the reason for the better adsorption of EBT onto UTG than ARS. Results from this investigation supported the efficiency of UTG as a low-cost and environmentally friendly solution for the adsorption of ARS and EBT from contaminated wastewater.

ARTICLE HISTORY
Received September 2, 2022
Accepted September 27, 2022
Published September 30, 2022

KEYWORDS
Adsorption, Typha grass, Alizarin Red S, Eriochrome Black T

© The authors. This is an Open Access article distributed under the terms of the Creative Commons Attribution 4.0 License (https://creativecommons.org/licenses/by-nc/4.0/)

INTRODUCTION

The global discharge of industrial effluents into the environment poses substantial risks by polluting the ecosystem. This condition is a major cause of degradation of surface water and groundwater resources (Rashidi *et al.*, 2019; Rashidi *et al.*, 2021). One of the main sources of pollution which has a negative impact on aquatic life as well as human health is the discharge of hazardous coloured effluents from various manufacturing industries into aquatic media (Ghaderpoori and Dehghani, 2016). Contamination of the water bodies is one of the major pollution source involving majority of the industries discharging dyes, heavy metals, pharmaceutical waste, and various other organic pollutants (Khan *et al.*, 2018). Even at minute concentrations, these contaminants are non-biodegradable and can cause genetic and physiological issues in living organisms (Fu and Wang, 2011).

Dyes are complicated coloured aromatic compounds which are mostly of synthetic origins (Rashidi *et al.*, 2021). Synthetic dyes are widely used in the textile industries because they structurally feature reactive functional groups with high fiber-binding properties (Bilal and Asgher, 2015). It is estimated that 80,000 tons of dyes are produced and consumed almost yearly, making synthetic dyes one of the most damaging pollutants (Rossella *et al.*, 2021). Furthermore, it is evident that, human exposure to dyes may have serious health consequences, including allergies, cancer, mutagenesis, and teratogens (Gupta *et al.*, 2015).

Thus, environmentally, it has become desirable to treat wastewater containing dyes from industries (Rashidi *et al.*, 2021). The adsorption method especially at low concentrations, is the most effective and economical way to treat wastewater containing dyes (Putro *et al.*, 2021). This method however depends on the adsorption capacity of the adsorbent under consideration (Putro *et al.* 2021).

Correspondence: Sani M. Department of Pure and Industrial Chemistry, Faculty of Physical Sciences, Bayero University, Kano, Nigeria. ✉ musaniyaya@gmail.com; Phone: (+234) 803 7733 519
How to cite: Ayuba, A. M. and Sani, M. (2022). Study on Adsorption of Alizarin Red S and Eriochrome Black T Dyes by Untreated Typha Grass as a Low Cost Adsorbent. UMYU Scientifica,1(1),155–165. https://doi.org/10.56919/usci.1122.020

This study aims to examine the adsorptive ability of untreated (raw) typha grass (UTG) by utilizing a batch adsorption approach for the decolourization of anionic dyes, ARS and EBT from wastewater. This grass was chosen because of its availability, affordability, and environmental friendliness (Taufiq *et al.*, 2018).

MATERIALS AND METHODS

General

The stock of chemicals used in this research were obtained from Sigma-Aldrich Ltd., London. These includes: Hydrochloric acid, sodium hydroxide, Alizarin Red S (ARS) dye and Eriochrome Black T (EBT) dye. The chemicals were used without further purification, and all solutions were prepared with distilled water. The scanning electron microscopy images were recorded using Phenom World Eindhoven microscope, while the Fourier Transformed Infrared Spectroscopy was recorded on Cary 630 FTIR Spectrophotometer from Agilent Technology. UV-Visible spectroscopy was performed on Perkin-Elmer Lambda 35 UV-Visible spectrometer.

Preparation of Dye Solutions

To make 1000 mg/L of the stock solution for each of the commercial grade Alizarin red S and Eriochrome black T dyes, 1g of each ARS and EBT dyes were weighed and dissolved differently into 1L volumetric flask and made up to the mark using distilled water. The stock solution was diluted with distilled water to prepare the experimental solutions at the desired concentration. Subsequently, the concentrations of the dyes solutions were measured using UV-Visible spectrometer (Perkin Elmer, Lambda 35) at maximum wavelengths of 424.89 nm and 524.44 nm for ARS and EBT, respectively. The chemical structure of the studied dyes is as presented in Figure 1.

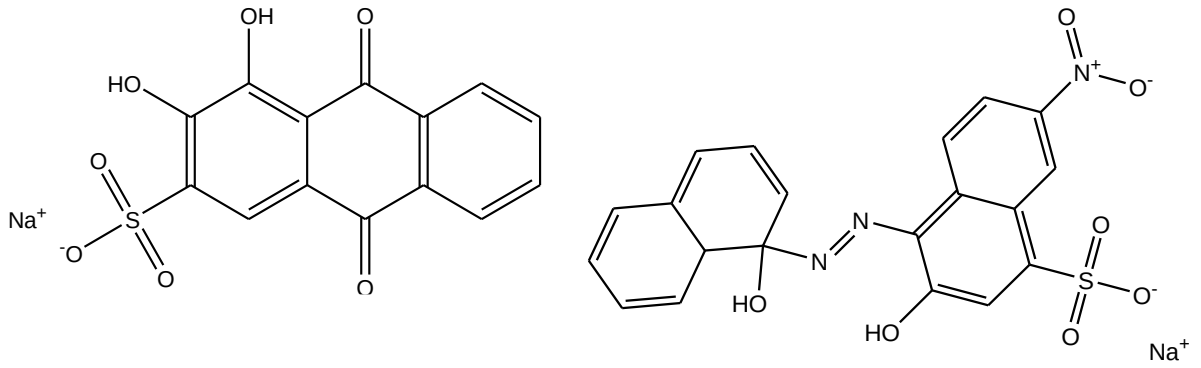

(a) Sodium3,4-dihydroxy-9,10-dioxoanthracene-2-sulfonate

(b) Sodium1-[1-hydroxynaphthylazo]-6-nitro-2-naphthol-4-sulfonate

Figure 1: Chemical Structures of (a) Alizarin Red S and (b) Eriochrome Black T Dyes

Preparation and Characterization of Typha Grass (UTG)

The typha grass was obtained from Marma town, Guri local government area of Jigawa State, Nigeria. The sample was first washed with tap water then distilled water to remove the impurities (Nwosu *et al.,* 2017). The sample was air-dried and then oven dried at 105^{0}C. The dried sample was untreated, pulverized and passed through a 2mm sieve.

The physical properties of the adsorbent, such as moisture content, bulk density, and pore volume, were determined using the methods reported by Ali *et al.* (2018); Ayuba and Idoko (2020). As reported by Bakatula (2018), the point of zero charge (PZC) of UTG was investigated using the salt addition method. The surface morphology before/after adsorption were studied using scanning electron microscopy (SEM). While the Fourier transformed infrared (FTIR) spectroscopy was also recorded both before and after dye adsorption.

Batch Adsorption Study

To find the ideal conditions for the equilibrium adsorption of ARS and EBT onto UTG, batch experiments were conducted and the optimized condition was found. Thus, in a 250 cm^3 conical flask, each system was operated independently at the temperature of 30^{0}C, 40^{0}C, and 50^{0}C. The conical flasks were covered during the equilibration period and set up on an Innova 4000 incubator shaker with temperature control for the optimal times. The substance was filtered through Whatman No 1 filter paper after attaining adsorption equilibrium. The filtrate was examined using UV-Visible spectrometer. Then the efficiency of the dyes to adsorb from their aqueous solutions onto UTG was calculated using equations 1 and 2 as reported by Bansal *et al.* (2020) and Ayuba and Idoko (2021).

$$\text{Adsorption Capacity (qe)} = \frac{(C_o - C_e)x\,V}{m} \quad (1)$$

$$\% \text{ Adsorption} = \left(\frac{C_o - C_e}{C_o}\right) \text{x } 100 \quad (2)$$

Where V is the volume of dye solution (L), m is the mass (g) of the adsorbent, and qe is the adsorption capacity (mg/g). Co and Ce are the initial and final equilibrium concentrations (mg/l) of the dyes in solution.

RESULTS AND DISCUSSION

Adsorbent Characterization

The physical characteristics of the adsorbent, including bulk density (organic matter), moisture content, and pore volume, are presented in Table 1. The results showed that the adsorbent exhibited good adsorptive properties for removing anionic dyes from aqueous solution owing to its low moisture content, high pore volume, and bulk density. Ayuba and Thomas (2021) reported similar results when they used carbonized Bambara groundnut (*Vigra subterranean*) shells to remove Paraquat dichloride from aqueous solution.

Table 1: Physical properties of untreated typha grass (UTG)

Moisture Content (%)	Bulk Density (gcm^{-3})	Pore Volume (cm^3)
17.80	0.397	1.253

Figure 2 shows the graph of the point of zero charge (PZC) for UTG adsorbent. Since there was no surface charge at the PZC that could be neutralized by ions at the adsorbent's surface, any adsorbed ions that do exist must be bonded in surface complexes. The pH of the neutral medium, or the region where the equilibrated ions in an aqueous solution are, is around 7, which indicates the presence of complete charge balance in the UTG under study. Moreover, substrates with low PZC values have the strongest tendency to treat effluents contaminated with cations, although the substrates with high PZC values would be better suited to adsorb anions (Nasiruddin and Anila, 2007; Zhang *et al.*, 2020).

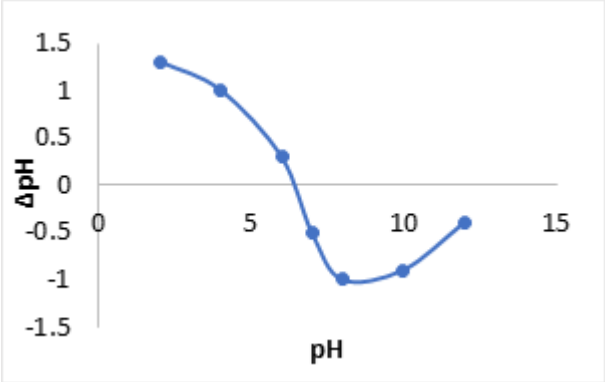

Figure 2: Measurement of point of zero charge (PZC) of UTG

The study of an adsorbent's surface morphology is essential in determining how well-suited it is to interact with the species it comes into contact with (Bansal *et al.*, 2020). Figure 3 gives the result of surface morphology analysis of UTG characterized by SEM methodology. SEM was employed to identify any surface morphological changes that might occur on UTG prior to and after the adsorption of ARS and EBT dyes. The instrument was operated at x500 magnification and a 15.00 kV accelerating voltage (Ali *et al.*, 2018). Whereas figure 3a indicates that the surface of UTG was rough, more porous, and more amorphous before the adsorption of each dye than it was after. In Figure 3b and c, earlier pores and rough surfaces in the un-adsorbed UTG have significantly decreased in comparison to Figure 3a because of the dyes' adsorption onto its surface. Secondly, it is obvious from comparing Figures 3b and c that EBT covers a greater proportion of UTG than ARS. Other authors have reported these observations as an indicator and evidence of adsorption of species onto adsorbents (Madhushika *et al.*, 2020).

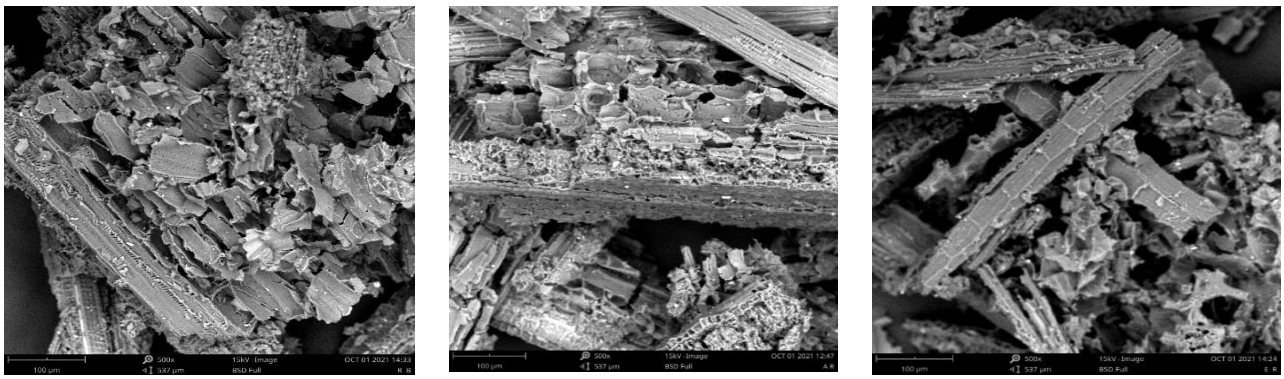

(a) **(b)** **(c)**

Figure 3: SEM micrographs of (a) UTG before adsorption and (b) after adsorption onto ARS and (c) after adsorption onto EBT.

FTIR was used to identify the functional groups that were present in the samples. Figures 4a–c illustrates the FTIR spectra of UTG both before and after ARS and EBT adsorption. The significant distinctive peaks

identified at 3327 cm^{-1}, 2918 cm^{-1}, 1607 cm^{-1}, 1514 cm^{-1}, and 1104 cm^{-1} before adsorption were connected to the stretching vibration mode of O-H, C-H, C=O, C≡C, and C-O groups, respectively (Ali, *et al.,* 2018). After loading UTG with ARS and EBT, there was a notable change in the vibration frequency of the free OH, C=O, and C-O stretches. Possible causes of the vibration frequency changes include the binding of ARS and EBT ions to the surface of the adsorbents (Babalola *et al.*, 2016). Because some of the important adsorption sites characteristics of effective adsorbents comprise hydroxyl, carbonyl, and carboxylic acid (Itodo *et al.*, 2011). The variation in absorption bands of the detected functional groups before and after adsorption were reported in Table 2. Different absorption bands were not witnessed before and after adsorption of the dyes onto UTG in C-H and C≡C stretches, an indication that they did not partake in the adsorption process. But those in O-H (for ARS) and C-O (for EBT) and C=O stretch (for both ARS and EBT) are indicators of the functional group likely used for the adsorption of the dyes onto UTG.

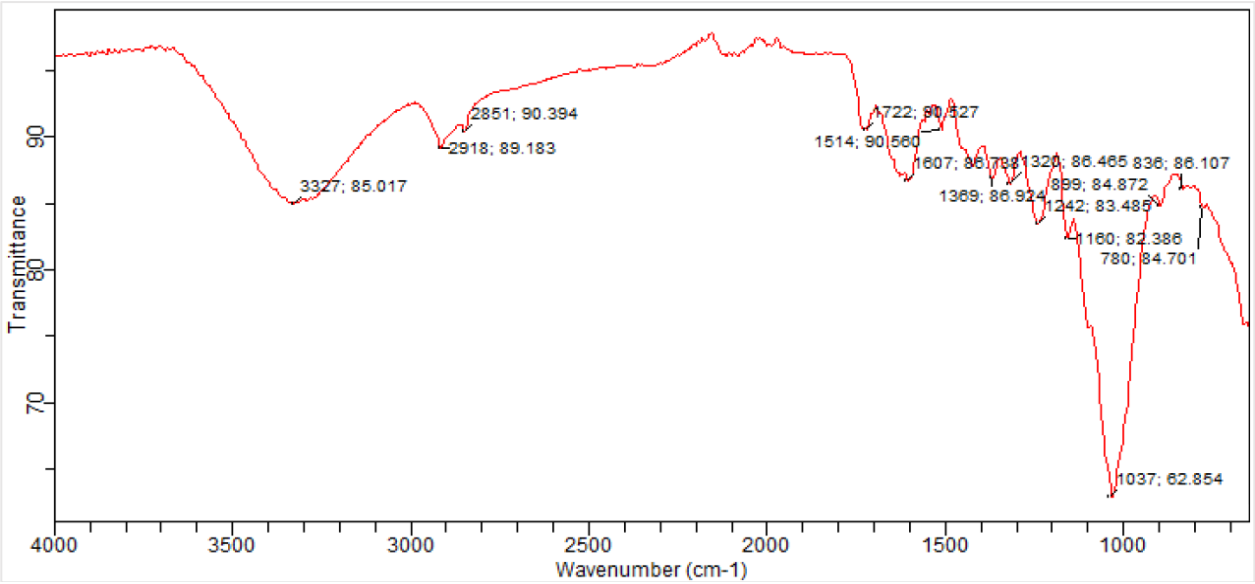

(a)

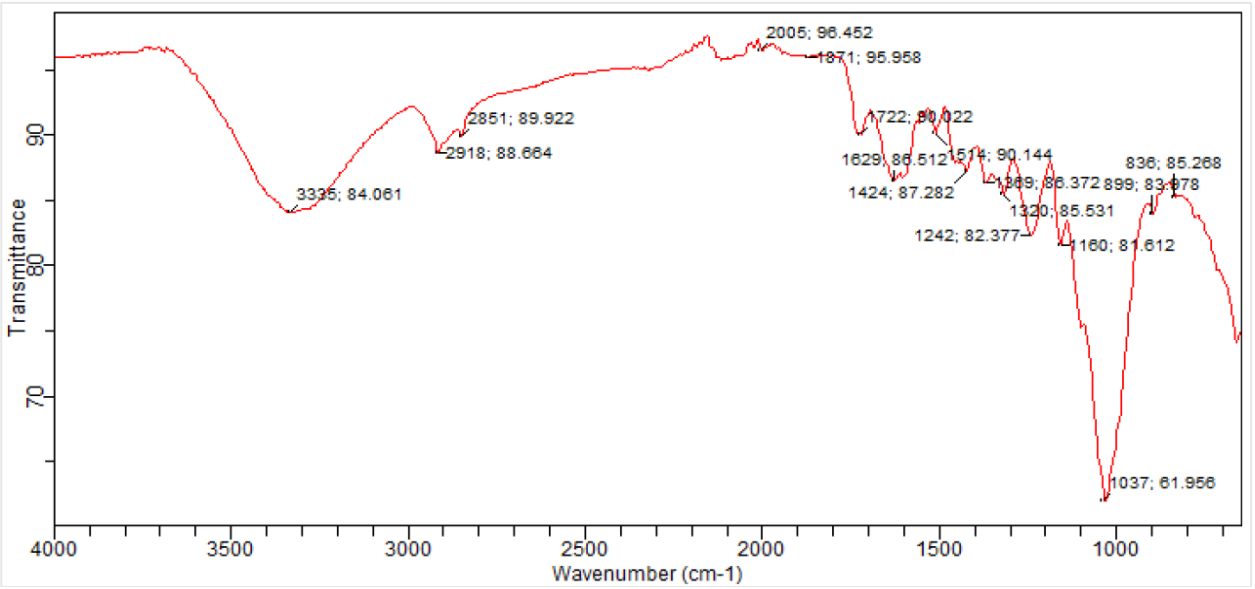

(b)

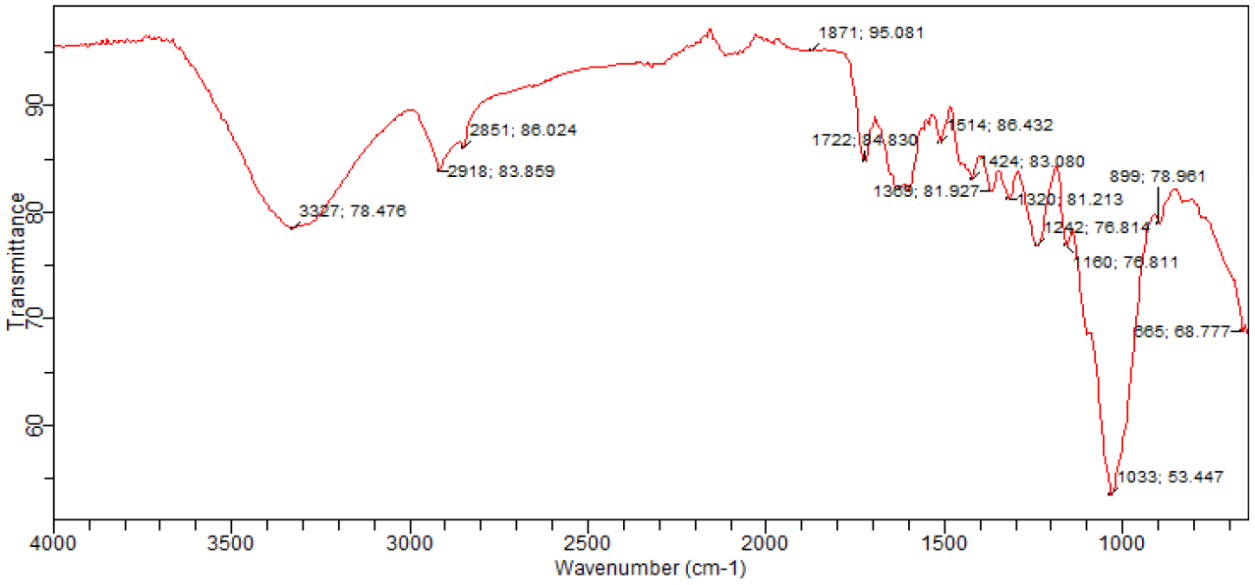

(c)

Figure 4: FTIR spectra of UTG (a) before adsorption (b) after ARS adsorption (c) after EBT adsorption.

Table 2: Summary of FTIR absorption bands of UTG before and after adsorption of ARS and EBT

Functional Group	Absorption range (cm^{-1})	Before absorption (cm^{-1})	After absorption onto ARS (cm^{-1})	Difference (cm^{-1})	After absorption onto EBT (cm^{-1})	Difference (cm^{-1})
OH stretch	3700-2500	3327	3335	13	3327	0
C-H stretch	3000-2840	2918	2918	0	2918	0
C=O stretch	1710-1580	1607	1629	12	1722	115
C≡C stretch	675-1550	1514	1514	0	1514	0
C-O stretch	1080-1300	1104	1104	0	1160	56

Batch Adsorption Studies

Effect of Contact Time

The influence of the contact time between 0-120 min of ARS and EBT removal by UTG was investigated in a suspension of 50 mg/L with 0.1g adsorbent at neutral pH. Adsorption happened rapidly at the beginning of the process until the equilibrium was reached within the first 10min for EBT and 15min for ARS (Figure 5a). During the duration, up to a maximum of 120 minutes, adsorption approached a constant condition. This optimum adsorption contact times were used for each of the dyes during batch adsorption studies. The abundance of unoccupied sites on an adsorbent's surface is connected to the rapid adsorption of dyes by the adsorbent at the beginning of contact time (Rashidi *et al.*, 2021). As the time progresses to a maximum, the unoccupied sites would then be filled with dye molecules, eventually leading to desorption (Nourmoradi *et al.*, 2012).

Effect of Adsorbent Dosage

The impact of the adsorbent dose (g) on the ARS and EBT dyes was investigated by adsorption experiments. The adsorption was conducted at neutral pH, room temperature, optimal contact time for each dye, dosage range of 0.02g-0.2g, initial dye concentration of 50 mg/L The adsorption capacity of ARS and EBT decreased as the adsorbent dose increased within the range of 0.02g-0.2g, attaining results of 49.92 mgg^{-1} and 47.43 mgg^{-1} for ARS and EBT, respectively (Figure 5b). Therefore, the highest adsorption capacity was obtained at a dosage of 0.02g of the adsorbent for both dyes. However, this dosage was chosen as the optimum rate for subsequent batch adsorption experiments. The availability of unoccupied active sites on the surface of the adsorbent was determined to be the main reason why the adsorption capacity of ARS and EBT increased. In comparison to substantially greater doses, the lowest dose (0.02g) was found to be more effective at adsorbing ARS and EBT (Bansal *et al.*, 2020). However, it was discovered in literature that as adsorbent dose increases, the effectiveness of the removal of dyes significantly improves (Li *et al.*, 2019). This behaviour is related to the large availability of empty adsorption sites during the initial stages of adsorption, followed by an increase in the repulsive forces brought on by the presence of the

adsorbed ions, making it more challenging to access the remaining sites (Nwosu *et al.*, 2017).

Effect of Initial Dye Concentration

The effect of the initial dye concentration in the range of 20-120 mg/L on the dye adsorption was investigated at room temperature and the contact time and adsorbent dosage were optimized. Figure 5c demonstrates a considerable increase in ARS and EBT adsorption with increasing initial dye concentration. The presence of more molecular ions in the solution, which compete with the available binding sites on the surface of the adsorbent, is responsible for this considerable change in the adsorption capacity of UTG with a rise in both ARS and EBT concentrations (Pahalagedara *et al.*, 2014). However, increase in ARS and EBT concentration undesirably affects the removal of the dyes. While the removal of ARS and EBT decreased as the initial dye concentration was increased from 20 to 120 mg/L (Liu *et al.*, 2015). The electrostatic attraction between the dye molecules in solution and the dye molecules adsorbed by the UTG is increased as the initial dye concentration increases.

Effect of pH

By varying the solution pH values from 2 to 10, the influence of pH on the adsorption of ARS and EBT onto the surface of UTG was evaluated. Figure 5d demonstrated that as the pH of the ARS solution increased, the adsorption capacity of UTG decreased as the pH of the EBT solution increased (Zubair *et al.*, 2017). Therefore, at pH levels of 8 and 2, respectively, the optimum adsorption capacity for ARS was 47.99 mg/g while for EBT was 49.44 mg/g. This outcome could be explained by variations in the adsorbent's surface charge. However, by lowering the pH of the solution, the amount of positive charges on an adsorbent's surface improves adsorption (Rashidi *et al.*, 2021); in the same way, it increased ARS's ability to adsorb in more acidic pH solutions. In other words, for EBT, the electrostatic repulsions between the negatively charged adsorbent and anionic dyes increased at a basic pH (Raveendra *et al.*, 2015).

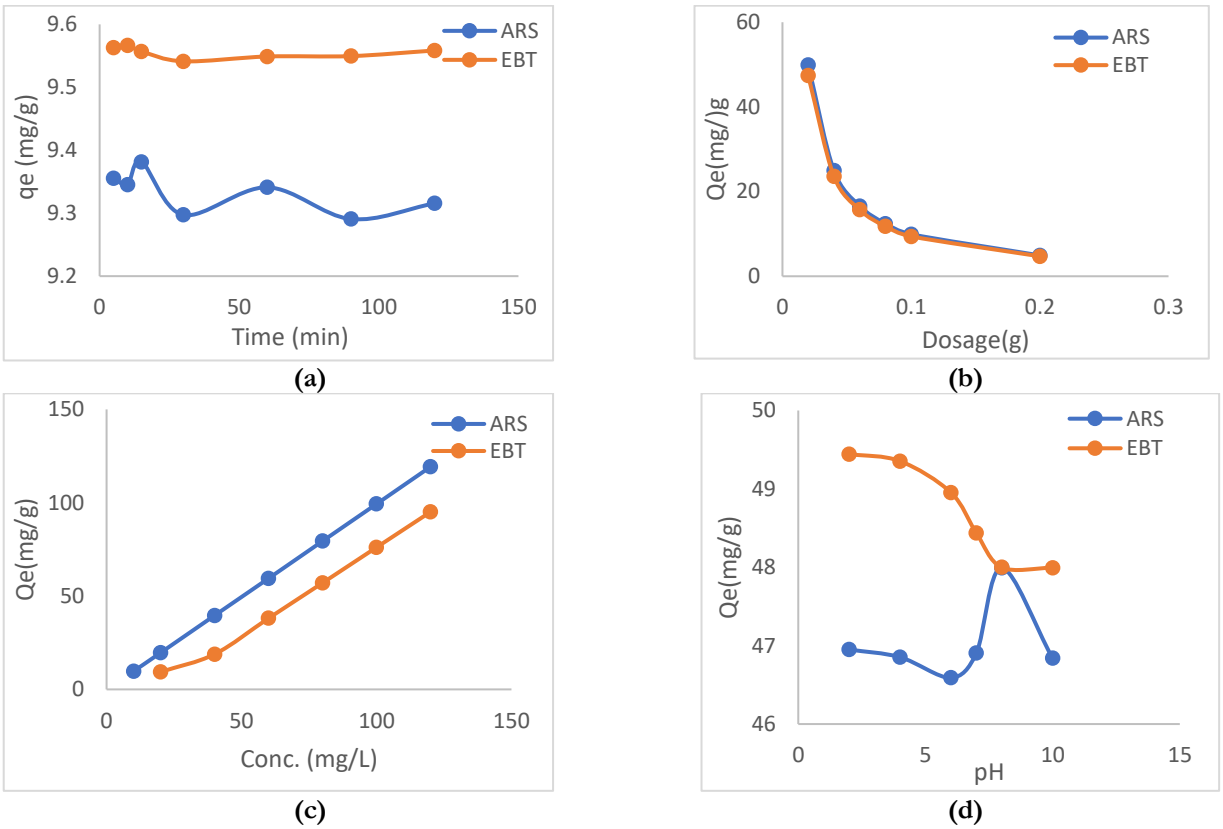

Figure 5. Effect of (a) contact time, (b) dosage, (c) initial dye concentration, (d) pH, on the adsorption of ARS and EBT onto UTG

Adsorption Isotherms

The adsorption isotherms are useful for determining how the adsorbate is distributed on the adsorbent's surface under equilibrium conditions (Sharma *et al.*, 2018). To identify the mechanistic characteristics of interactions between the adsorbent and the adsorbate at equilibrium, Langmuir, Freundlich, Temkin, and D-R models were tested (Bansal *et al.*, 2020). The models were employed to evaluate the removal of ARS and EBT by UTG. The linearized form of these models are presented in equations (3-6) as reported by Sadani *et al.* (2020).

$$\frac{1}{q_e} = \frac{1}{Q_o} + \frac{1}{Q_o K_L C_e} \qquad \text{Langmuir} \qquad (3)$$

$$LogQ_e = logK_f + \frac{1}{n}logC_e \quad \text{Freundlich} \quad (4)$$

$$q_e = B_T lnC_e + B_T lnK_T \quad \text{Temkin} \quad (5)$$

$$lnq_e = lnq_m - \beta\varepsilon^2 \quad \text{Dubining Radushkevich (D-R)} \quad (6)$$

Where Ce stands for the equilibrium dye concentration (mg/L); qe and Qo for the equilibrium and maximum adsorption capacities (mg/g); and K_L, K_F, K_T, and β for the Langmuir, Freundlich, Temkin, and D-R constants, respectively. The intensity of the bond and the value of n indicate that ARS and EBT can be successfully adsorbed onto UTG (Nourmoradi *et al.*, 2015). Table 3 displays the calculated values of the isotherm parameters for ARS and EBT removal by UTG.

Table 3: Adsorption Isotherm constants for the adsorption of ARS and EBT onto UTG

Parameter	Alizarin Red S	Eriochrome Black T
Langmuir		
Q_O(mg/g)	-9.3720	-151.51
K_L(L/mg)	-0.1680	-0.091
R_L	-0.1115	-0.222
R^2	0.967	0.994
Freundlich		
1/n	1.0029	1.1421
n	0.4992	0.8755
K_F	1.2083	16.270
R^2	0.958	0.990
Temkin		
A_T	0.5288	1.445
b_T	86.09	53.415
B	29.259	47.161
R^2	0.827	0.92
Dubinin-Radushkevich		
q_m(mg/g)	48.638	85.567
K_{dr}(mol²/KJ²)	3.0×10^{-6}	4.0×10^{-6}
E(kJ/mol)	4.0×10^{-1}	1.12×10^{10}
R^2	0.841	0.901

However, from the results obtained, the Freundlich isotherm established a greater correlation coefficient (R^2) value than Langmuir, Temkin and D-R isotherms. Thus, it can be said that the Freundlich isotherm model provided the greatest match for the experimental data of ARS and EBT removal by the UTG (Zhou *et al.*, 2018). This suggests that the physical adsorption process is in control of the adsorption of ARS and EBT dyes using UTG as an adsorbent and validates the existence of heterogeneous adsorption sites on UTG (Ahmed *et al.*, 2021). Furthermore, the obtained result revealed that the removal of ARS and EBT by a variety of adsorbents, including modified kaolinite clay, $NiFe_2O_4$ magnetic nanoparticles, and Mosambi peel activated carbon, follows a similar isotherm model as reported by Zong *et al.*, (2016) and Sharma *et al.*, (2018).

Kinetic Studies

Data from batch adsorption studies were tested against four kinetic models in order to understand the adsorption kinetics of ARS and EBT dyes onto UTG. These includes kinetic explanations of the adsorption of these dyes onto UTG adsorbent using pseudo-first-order, pseudo-second-order, Elovich, and intraparticle diffusion (Alinejad *et al.*, 2019). The kinetics models employed have a linear form as shown in equations (7–10) as reported by Ayuba *et al.* (2020) and Kamarehie *et al.* (2020).

$$\log(q_e - q_t) = \log(q_e) - \frac{k_1}{2.303}t \ (\text{Pseudo} - \text{First order}) \quad (7)$$

$$\frac{t}{q_t} = \frac{1}{k_2 q_e^2} + \frac{1}{q_e}(t) \quad (\text{Pseudo} - \text{Second order}) \quad (8)$$

$$q_t = {}^{1}/_{\beta}\ln(\alpha\beta) + \left({}^{1}/_{\beta}\right) lnt \quad (\text{Elovich}) \quad (9)$$

$$q_t = C + K_{int}t^{1_2} \quad (\text{Intraparticle Diffusion}) \quad (10)$$

Where q_e and q_t stand for the quantity of adsorption at equilibrium and at the time, t, and k_1, k_2 and k_{int} stand for the pseudo-first order, pseudo-second order, Elovich and Intraparticle diffusion rate constants, respectively. However, Table 4 givess the kinetics of the ARS and EBT adsorption onto UTG as well as the values of the rate constants and q_e as determined by the pseudo-first, pseudo-second order, Elovich and Intraparticle diffusion. Furthermore, the results from the aforementioned models showed that, in comparison to other models considered, the correlation coefficient value (R^2) favoured by pseudo-second order. Additionally, the pseudo second order model kinetics used to describe the ARS and EBT adsorption by UTG can also clearly be seen when comparing the qe_{Cal} and qe_{Exp} of the tested models (Li *et al.*, 2019; Yao *et al.*, 2020).

Table 4: Kinetic models for the adsorption of ARS and EBT onto UTG

Pseudo-first order	Parameter	qe_{Cal}(mg/g)	qe_{Exp}(mg/g)	K_1(min⁻¹)	R^2
	ARS	46.682	0.328	0.019	0.120
	EBT	49.511	0.124	0.006	0.004
Pseudo-second order	Parameter	qe_{Cal}(mg/g)	qe_{Exp}(mg/g)	K_2(min⁻¹)	R^2
	ARS	46.682	46.511	0.770	0.999
	EBT	49.511	49.504	0.020	0.998

Table 4: Continued

Elovich	Parameter	B	A	R^2
	ARS	178.571	1.2×10^{81}	0.039
	EBT	68.493	4.1×10^{171}	0.011
Intraparticle diffusion	Parameter	K_3	C	R^2
	ARS	0.004	46.508	0.142
	EBT	-0.015	12.02	0.001

Thermodynamic Studies

Thermodynamic studies provide vital information on the energetics associated with the adsorption process. The thermodynamics of an adsorption process can be explained using the changes in enthalpy (ΔH), entropy (ΔS) and Gibb's free energy (ΔG). Three different temperatures (298K, 308K and 318K) were used for the batch adsorption studies. Equation (11) was used to determine how the Gibb's free energy changed for the adsorption. Equation (12) was used to calculate the changes in entropy and enthalpy by plotting $\ln K_L$ against 1/T to give Van't Hoff's plot (Figure 6). ΔH was calculated using the graph's slope, whereas ΔS was calculated using the plot's intercept (Min *et al.*, 2012; Umar *et al.*, 2021).

$$\Delta G = -RT\ln K_L \quad (11)$$

$$\ln K_L = \frac{\Delta H}{RT} + \frac{\Delta S}{R} \quad (12)$$

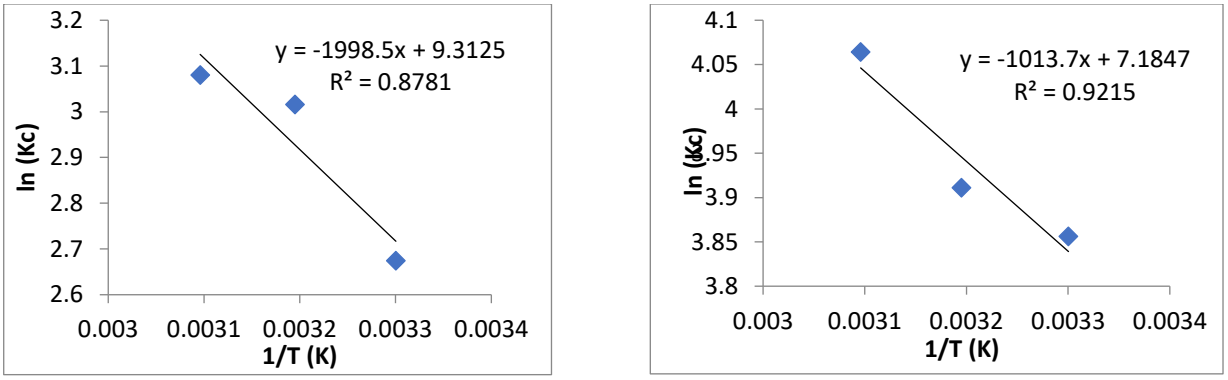

(a) **(b)**

Figure 6: Van't Hoff plot for (a) ARS and (b) EBT adsorption at different temperatures

Summary of the results obtained from the thermodynamic evaluation are as presented in table 5. The adsorption system was thermodynamically feasible and spontaneous due to the negative values of ΔG, and with values lower than -20KJ/mol, the adsorption process for both dyes was physical in nature (Nourmoradi *et al.*, 2015; Ayuba and Idoko, 2020). As the temperature increases from 298 to 318K, the rate of adsorption increased. Furthermore, the endothermic nature of the adsorption of ARS and EBT by UTG was confirmed by the positive value of enthalpy change ΔH. In addition, the results showed that the ΔH values were positive and lower than 80 kJ/mol, indicating that the adsorbate and adsorbent surface were physically interacting during the adsorption process. Moreover, positive entropy change (ΔS) values indicated that UTG can easily loose off ARS and EBT and that the adsorption phenomena is entropy-controlled rather than enthalpy-controlled (Asadullah *et al.*, 2019).

Table 5: Thermodynamic parameters for the adsorption of ARS and EBT onto UTG

Dye	T (K)	K_c	ΔG (KJ/mol)	ΔH (KJ/mol)	ΔS (J/mol.K)
ARS	303	14.503	-6.737	16.616	77.424
	313	20.399	-7.847		
	323	21.757	-8.271		
EBT	303	65.439	-10.177	8.283	53.819
	313	49.018	-10.532		
	323	98.901	-12.337		

CONCLUSION

In this study, anionic dyes ARS and EBT were extracted from aqueous solution using a batch method, and UTG was employed as a cheap, eco-friendly and cost-effective adsorbent. Some physical parameters of the adsorbent were analysed and found the adsorbent to be promising. The surface of the adsorbent was characterized in order to assess the extent of interaction between studied dyes and the surface. The batch system performance was optimized based on how the contact time, adsorbent dose, initial dye concentration, temperature and pH affect adsorption efficiency. The pseudo-second-order kinetic and Freundlich isotherm models performed well in describing the experimental data for both dyes, according to the results. The adsorption process was thermodynamically feasible, spontaneous and adhered to the physical adsorption of dyes mechanism. Maximum adsorption capacity obtained for ARS and EBT were 47.99 mg/g and 49.44 respectively. This is an indication that EBT was better adsorbed than ARS even though they were both anionic in nature. Presence of diazo and nitro functional groups in EBT in addition to hydroxyl and sulphate functional groups present in ARS may be the reason for the better adsorption of EBT onto UTG over ARS. The findings showed how successfully UTG may be utilized to remove anionic dyes from aqueous medium. Specifically, the findings suggested that UTG might prove to be a useful adsorbent for the treatment of ARS and EBT-contaminated water.

ACKNOWLEDGEMENT

The analysis of the adsorbent before and after adsorption with respect to FT-IR and SEM was conducted by the staff of Central Laboratory Complex, Bayero University, Kano and they are well appreciated.

CONFLICT OF INTEREST

The authors state that they are free of any conflicts of interest that might have affected the work presented for the current study.

REFERENCES

Ahmed, A., Ali, A., Ahmed, M., Parida, K. N., Ahmad, A. J. S. and Ahmad, P. (2021). Technology, Construction and topological studies of a three dimensional (3D) coordination polymer showing selective adsorption of aromatic hazardous dyes. *Separation and Purification Technology,* 265, 118482. **[Crossref]**

Ali, I., Peng, C., Ye, T. and Naz, I. (2018). Sorption of cationic malachite green dye on phytogenic magnetic nanoparticles functionalized by 3-marcaptopropanic acid. *Journal of Royal Society of Chemistry Advances,* 8, 8878-8897. **[Crossref]**

Alinejad, A., Akbari, H., Ghaderpoori, M., Jeihooni, A. K. and Adibzadeh, A. (2019). Catalytic ozonation process using MgO nano-catalyst to degrade methotrexate from aqueous solutions and cytotoxicity studies in human lung epithelial cells (A549) after treatment. *Journal of Royal Society Chemistry Advances*, 9, 8209. **[Crossref]**

Asadullah, A., Kaewsichan, L. and Tohdee, K. (2019). Adsorption of hexavalent chromium onto alkali-modified biochar derived from Lepironia articulata: A kinetic, equilibrium, and thermodynamic study. *Water Environment Research,* 1-14. **[Crossref]**

Ayuba, A. M., Ladan, M. and Muhammad, A. S. (2020). Thermodynamic and kinetic study of Pb (II) amputation by river sediment. *Applied Journal of Environmental Engineering Science,* 6(3), 213-226.

Ayuba, A. M. and Idoko, B. (2020). Kinetic, equilibrium and thermodynamic studies on the adsorption of crystal violet dye from aqueous solution using activated cowpea (*Vigna Unguiculata)* husk. *Applied Journal of Environmental Engineering Science,* 6(2), 182-195.

Ayuba, A. M. and Idoko B. (2021). Cowpea husk adsorbent for the removal of crystal violet dye from aqueous solution. *Arabian Journal of Chemical and Environmental Research,* 8(1), 114–132.

Ayuba, A. M. and Thomas, N. A. (2021). Paraquat dichloride adsorption from aqueous solution using carbonised Bambara groundnut (*Vigra subterranean*) shells. *Bayero Journal of Pure and Applied Sciences,* 12(1), 167-177. ISSN 2006-6996. **[Crossref]**

Babalola, J. O., Olowoyo, J. O., Durojaiye, A. O., Olatunde, A. M., Unuabonah, E. I. and Omorogie, M. O. (2016). Understanding the removal and regeneration potentials of biogenic wastes for toxic metals and organic dyes. *Journal of Taiwan Institute of Chemical Engineers,* 58, 490–499. **[Crossref]**

Bakatula, E. N., Richard, D., Neculita, C. M., Zagury, C. M. and Gerald, J. (2018). Determination of point of zero charge of natural organic materials. *Environmental Science and Pollution Research,* 25, 7823-7833. **[Crossref]**

Bansal, M., Patnala, P. K. and Dugmore, T. (2020). Adsorption of Eriochrome Black-T (EBT) using tea waste as a low cost adsorbent by batch studies: A green approach for dye effluent

treatments. *Current Research in Green and Sustainable Chemistry,* 3, 100036. **[Crossref]**

Bilal, M. and Asgher, M. (2015). Sandal reactive dyes decolorization and cytotoxicity reduction using manganese peroxidase immobilized onto polyvinyl alcohol-alginate beads. *Chemistry Central Journal,* 9, 47-52. **[Crossref]**

Fu, F. and Wang, Q., (2011). Removal of Heavy Metal Ions from Wastewaters: a review. *Journal of Environmental Management,* 92, 407–418. **[Crossref]**

Ghaderpoori, M. and Dehghani, M. H. (2016). Investigating the removal of linear alkyl benzene sulfonate from aqueous solutions by ultraviolet irradiation and hydrogen peroxide process. *Desalination and Water Treatment*, 57, 15208. **[Crossref]**

Gupta, V., Agarwal, A. and Singh, M. (2015). Belpatra (Aegel Marmelos) Bark Powder as an Adsorbent for the Color Removal of Textile Dye "Torque Blue". *International Journal of Engineering, Science and Technology,* 4, 56. **[Crossref]**

Itodo, U., Usman A. and Ugboaja, C. (2011). A Rate Study of Received and Derived Activated Carbon and Pseudo Constants for Methyl Red Sorption. *Journal of Encapsulation and Adsorption Sciences,* 1, 57- 64. **[Crossref]**

Kamarehie, B., Tizabi, S. M. S., Heydari, R., Sadeghi, S., Ghaderpoori, M., Ghaderpoury, A. and Alinejad, A. (2020). Catalytic ozonation process using MgO-PAC to degrade bisphenol A from aqueous solutions. *Desalination and Water Treatment,* 184, 232. **[Crossref]**

Khan, S., Sayed, M., Sohail, M. and Shah, L. A. (2018). Advanced Oxidation and Reduction Processes. Advances in Water Purification Techniques: Meeting the Needs of Developed and Developing Countries, Elsevier Incorporation. pp. 135–164. **[Crossref]**

Li, C., Zhang, N., Jixiao, C., Jiawen, J., Liu, X., Wang, J., Zhu, J. and Ma, Y. (2019). Temperature and pH sensitive composite for rapid and effective removal of sulfonylurea herbicides in aqueous solution. *Journal of Environmental Pollution,* 255, 113150. **[Crossref]**

Liu, Q., Yang, B., Zhang, L. and Huang, R. (2015). Adsorption of an ionic azo dye by cross-linked chitosan/bentonite composite. *International Journal of Biological Macromolecul,* 72, 1129–1135. **[Crossref]**

Madhushika, H. G., Ariyadasa, T. U. and Gunawardena, S. H. P. (2020). Biological decolourization of textile industry wastewater by a developed bacterial consortium. *Water Science Technology,* 80, 1910–1918. **[Crossref]**

Martínez-Huitle, C. A. and Brillas, E. (2009). Decontamination of wastewaters containing synthetic organic dyes by electrochemical methods: A general review. *Applied Catalysis B: Environmental Journal,* 87, 105–145. **[Crossref]**

Min, M., Shen, L., Hong, G., Zhu, M., Zhang, Y., Wang, X., Chen, Y. and Hsiao, B.S. (2012). Micronano structure poly(ether sulfones)/poly(ethyleneimine) nanofibrous affinity membranes for adsorption of anionic dyes and heavy metal ions in aqueous solution. *Chemical Engineering Journal*, 197, 88-100. **[Crossref]**

Nasiruddin, K. and Anila, S. (2007). Determination of points of zero charge of natural and treated adsorbents. *Surface Review and Letters (SRL)*, 14(3), 461–469. **[Crossref]**

Nourmoradi, H., Ghiasvand, A. and Noorimotlagh, Z. (2015). Removal of methylene blue and acid orange 7 from activated carbon coated with zinc oxide (ZnO) nanoparticles: equilibrium, kinetic and thermodynamic study. *Desalination and Water Treatment*, 55, 252. **[Crossref]**

Nourmoradi, H., Khiadani, M. and Nikaeen, M. (2012). Removal of benzene, Toluene, Ethylbenzene and Xylene (BTEX) from aqueous solutions by Montmorillonite modified with non-ionic surfactant: Equilibrium, Kinetic and Thermodynamic study. *Chemical Engineering Journal,* 191, 341-348. **[Crossref]**

Nwosu, F. O., Adekola, F. A. and Salami, A. O. (2017). Adsorption of N-nitrophenol (PNP) Using Pilli nut shell action. *Pakistani. Journal of Analytical Environmental Chemistry,* 18(1), 69. **[Crossref]**

Pahalagedara, M. N., Samaraweera, M., Dharmarathna, S., Kuo, C. H., Pahalagedara, L. R., Gascón, J. A. and Suib, S. L. (2014). Removal of Azo Dyes: Intercalation into Sonochemically Synthesized NiAl Layered Double Hydroxide. *The Journal of Physical Chemistry,* 1(18), 17801-17809. **[Crossref]**

Putro, J. N., Yi-Hsu, J., Felycia, E. S., Shella, S. P. and Suryadi, I. (2021). Biosorption of dyes. *Green Chemistry and Water Remediation,* 5(3), 67-84. **[Crossref]**

Rashidi, R., Khaniabadi, Y. O. and Ghaderpoori, M. (2021). Adsorption of Eriochrome black-T from aqueous environment by raw Montmorillonite. *International Journal of Environmental Analytical Chemistry*. **[Crossref]**

Rashidi, R., Yousefinejad, S. and Mokarami, H. (2019). Catalytic ozonation using CuO/Clinoptilolite zeolite for the removal of formaldehyde from the air stream. *International Journal of Environmental Science Technology,* 16, 6629. **[Crossref]**

Raveendra, R. S., Prashanth, P. A., Malini, B. R. and Nagabhushana, B. M. (2015). Adsorption of Eriochrome black-T azo Dye from Aqueous solution on Low cost Activated Carbon prepared from Tridax procumbens. *Research Journal of Chemical Sciences,* 5(3), 9-13.

Rossella, G., Davide, D., Luca, T., Edmond, M. and Andrea, S. (2021). Adsorption of Malachite Green and Alizarin Red S Dyes Using Fe-BTC Metal Organic Framework as Adsorbent. *International Journal of Molecular Sciences,* 22, 788. **[Crossref]**

Sadani, M., Rasolevandi, T., Azarpira, H., Mahvi, A.H., Ghaderpoori, M., Mohseni, S. M. and Atamaleki, A. (2020). Arsenic selective adsorption using a nonomagnetic ion imprinted polymer: Optimization, equilibrium, and regeneration studies. *Journal of Molecular Liquid,* 317, 114246. **[Crossref]**

Sharma, S., Hasan, A., Kumar, N. and Pandey, L. M. (2018). Removal of methylene blue dye from aqueous solution using immobilized Agrobacterium fabrum biomass along with iron oxide nanoparticles as biosorbent. *Environmental Science and Pollution Research,* 1(22), 21605–21615, 25. **[Crossref]**

Taufiq, A., Hidayat, P. and Hidayat, A. (2018). Modified coal fly ash as low cost adsorbent for removal reactive dyes from batik industry. MATEC Web Conference. 154, 01037. **[Crossref]**

Umar, Y., Abdulrahman, I. K., Yusuf, A., Tahir, A. and Musa, H. (2021). Hexavalent chromium removal from simulated wastewater using biomass-based activated carbon: kinetics, mechanism, thermodynamics and regeneration studies. *Algerian Journal of Engineering and Technology,* 04, 030–044.

Yao, X., Ji, L., Guo, J., Ge, S., Lu, W., Chen, Y., Cai, L., Wang, Y. and Song, W. (2020). An abundant porous biochar material derived from wakame (*Undaria pinnatifida*) with high adsorption performance for three organic dyes. *Bioresource Technology,* 318, 124082. **[Crossref]**

Zhang, B. L., Qiu, W., Wang, P. P., Liu, Y. L., Zou, J., Wang, L. and Ma, J. (2020). Mechanism study about the adsorption of Pb(II) and Cd(II) with iron-trimesic metal-organic frameworks. *Chemical Engineering Journal,* 385, 123507. **[Crossref]**

Zhou, Y., Hu, Y., Huang, W., Cheng, G., Cui, C. and Lu, J. (2018). A novel amphoteric cyclodextrin-based adsorbent for simultaneous removal of cationic/anionic dyes and bisphenol A. *Chemical Engineering Journal,* 341, 47–57. **[Crossref]**

Zong, E., Liu, X., Jiang, J., Fu, S. and Chu, F. (2016). Preparation and characterization of zirconia-loaded lignocellulosic butanol residue as a biosorbent for phosphate removal from aqueous solution. *Applied Surface Science Journal,* 30(387), 419–430. **[Crossref]**

Zubair, M. N., Jarrah, S. A., Manzar, M., Al-Harthi, M., Daud, N. D., Mu'azu, S. and Haladu, A. (2017). Adsorption of Eriochrome Black T from Aqueous Phase on MgAl-, CoAl and NiFe-Calcined Layered Double Hydroxides: Kinetic, Equilibrium and Thermodynamic Studies. *Journal of Molecular Liquids,* S0167-7322(16)33014-8. **[Crossref]**